Electronic structure of epsilon-Ti_2N and delta'-Ti_2N

1993 J. Phys.: Condens. Matter 5 5261

(http://iopscience.iop.org/0953-8984/5/30/006)

J. Phys.: Condens. Matter 5 (1993) 5261–5276. Printed in the UK

Electronic structure of ϵ-Ti_2N and δ'-Ti_2N

R Eibler

Institute of Physical Chemistry, University of Vienna, A-1090 Wien, Währingerstraße 42, Austria

Received 8 March 1993, in final form 29 April 1993

Abstract. Self-consistent band structure calculations have been performed for the antirutile structure of ϵ-Ti_2N and for the metastable long-range ordered defect structure of δ'-Ti_2N. In accordance with recent neutron diffraction data a relaxation of the Ti atoms in direction of the crystallographic c-axis away from the vacancies was assumed. Band structures, densities of states, partial local densities of states and charge density contour plots are discussed with regard to the chemical bonding in these compounds. On the basis of the band structure data, a qualitative explanation for the occurrence of the metastable long-range ordered δ'-phase in the Ti–N_x system near a composition $x = 0.5$ and for the high stability of the ϵ-phase can be given. Contrary to hypothetically ordered $TiN_{0.75}$, no so-called vacancy states with σ bonding of Ti e_g-like states across the vacancies are found for δ'-Ti_2N.

1. Introduction

Titanium nitride crystallizes in the sodium chloride structure (δ-phase) over a wide range of composition ($TiN_{0.42}$ to $TiN_{1.02}$) [1]. Several versions of the phase diagram of TiN exist in the literature [2], with different values for the limiting N concentration of the δ-phase. By annealing TiN_x samples with $0.5 < x < 0.6$ at 773 K a tetragonal, long-range ordered defect structure of nominal composition Ti_2N, the so-called δ'-Ti_2N, is obtained [3–5], which can be derived from the sodium chloride structure by assuming long-range order of the vacancies on the N sublattice and by allowing for a shift of the Ti atoms along the fourfold tetragonal axis. A shift of the Ti atoms away from the vacancy [3, 5] as well as towards the vacancy [4] can be found in the literature. In the latest neutron diffraction experiments [5] a shift of 0.123 Å directed away from the vacancy has been measured. We based our band structure calculations on this value which we took to be the most reliable. The tetragonal unit cell of δ'-Ti_2N from [5] is shown in figure 1. It corresponds to a nominal composition Ti_8N_4 of four formula units Ti_2N. However, for the calculation a smaller rhombohedral unit cell accomodating two formula units of Ti_2N proves to be sufficient.

We have already calculated the electronic structure of stoichiometric TiN [6] and of the hypothetically ordered substoichiometric titanium nitride of composition $TiN_{0.75}$ [7], investigating especially the influence of the N vacancy on the electron density and the chemical bonds in its surrounding. These aspects cannot be treated by means of the KKR-CPA (Korringa–Kohn–Rostoker-coherent potential approximation) calculations for TiN_x where the vacancies are assumed to be disordered on the N sublattice [8, 9]. As the hypothetically ordered compound Ti_4N_3 of composition $TiN_{0.75}$ does not exist, it seemed interesting to calculate the band structure, density of states and electron density of a real ordered defect structure such as δ'-Ti_2N.

0953-8984/93/305261+16$07.50

However, δ'-Ti_2N is a metastable phase [10, 11] and transforms slowly upon aging into the stable, tetragonal ϵ-Ti_2N crystallizing in the antirutile structure [12]. ϵ-Ti_2N is also formed directly from disordered δ-$TiN_{0.5}$ at higher temperatures (about 900 K) [3]. The formation of the thermodynamically stable ϵ-phase is kinetically hindered and necessitates a high activation energy [13].

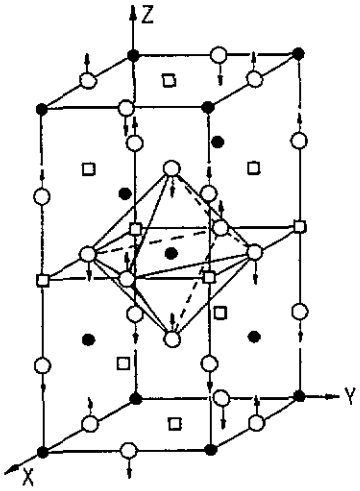

Figure 1. Tetragonal unit cell of δ'-Ti_2N with crystallographic axes X, Y and Z. Empty circles: Ti atoms; full circles: N atoms; squares: N vacancies. Atomic positions as given in table 2.

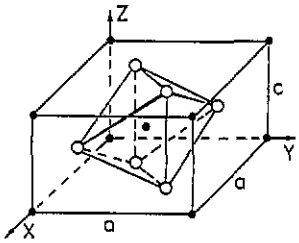

Figure 2. Unit cell of ϵ-Ti_2N with crystallographic axes X, Y and Z. Empty circles: Ti atoms; full circles: N atoms. Atomic positions as given in table 2.

The unit cell of ϵ-Ti_2N accommodating four Ti and two nitrogen atoms is shown in figure 2.

In both δ'- and ϵ-Ti_2N, each N atom is surrounded by a slightly distorted octahedron of Ti atoms (also shown in figures 1 and 2) with two Ti atoms at a smaller N–Ti distance than the other four. Thus, for ϵ-Ti_2N, the N–Ti bond distances are 2.07 Å, and 2.082 Å, and for δ'-Ti_2N 2.072 Å, and 2.078 Å (with the Ti atoms shifted away from the vacancy as found by Christensen *et al* [5]; a shift towards the vacancies as claimed in [4] would increase the difference between the N–Ti distances in δ'-Ti_2N considerably). These values must be compared to the nearest neighbour N–Ti distance of 2.12 Å, in stoichiometric, cubic δ-TiN and of 2.11 Å, in disordered δ-$TiN_{0.5}$ [1]. The smaller N–Ti bond length in the heminitrides indicates stronger N–Ti bonds in these compounds compared to cubic δ-TiN. The distance of the Ti atoms from the vacancies in δ'-Ti_2N is much larger in the Z-direction (2.32 Å) than in the X- or Y-direction (2.078 Å) if the shift of the Ti atoms away from the vacancies as found in [5] is assumed to be correct.

The distorted Ti octahedra are connected in a different way in the two heminitrides. For ϵ-Ti_2N, the octahedra centred at (000) and $(\frac{1}{2}, \frac{1}{2}, \frac{1}{2})$ differ in orientation by a 90° rotation about the crystallographic Z-axis with the titanium atoms forming a hexagonal close-packed sublattice where half of the octahedral interstitial sites are filled by N atoms. The formation of the antirutile structure of ϵ-Ti_2N can be visualized as starting with ribbons of these octahedra, each sharing two edges and aligned parallel to the principal axis. These ribbons are joined at the corners of the octahedra by rotating each ribbon about the Z-axis followed by a translation of $\frac{1}{2}(a, a, c)$. Thus, the ribbons of Ti octahedra in ϵ-Ti_2N share only vertices

in the basal plane. In δ'-Ti_2N the same distorted Ti octahedra are all oriented parallel to the Z-axis and share all their edges. Half of the octahedral interstitial sites occupied by N atoms remain vacant. The δ'-structure can also be imagined as built up from parallel ribbons of Ti octahedra around the N atoms. The octahedra of adjacent ribbons are only connected by weak Ti–Ti bonds between the Ti atoms surrrounding the vacancies.

The following paper will present band structure results for both ϵ- and δ'-Ti_2N.

After some computational aspects in section 2, section 3 presents eigenvalues, band structures (3.1), densities of states (DOS) (3.2), partial local charges and electron density contour plots (3.3) for both compounds. These results will be discussed in section 4. The energetic aspects will be left for a forthcoming paper [14].

2. Computational aspects

We employed the self-consistent LAPW (linearized augmented plane wave) method [15–17] for the band structure calculations, using the muffin-tin approximation for the potential, but allowing for the warping of the electron density by Fourier expanding the interstitial electron density in the SCF procedure. Muffin-tin spheres with the N muffin-tin radius were also positioned at the unoccupied N sublattice sites of δ'-Ti_2N. As in [7], the electron density inside the vacancy muffin-tin sphere was constructed by superposing the tails extending into the vacancy spheres of the wavefunctions centred at the adjacent atoms. Further details on the computation can be found in table 1.

Table 1. Computational details.

	ϵ-Ti_2N	δ'-Ti_2N
Method	Scalar-relativistic self-consistent LAPW [15, 16]	
Potential	Muffin-tin	
Electron density	Warped muffin-tin	
Exchange potential	Hedin–Lundqvist [18]	
Method for calculation of DOS	Tetrahedron method [19]	
k-expansion of wave function	Up to 465 k	Up to 490 k
l_{max} inside muffin-tin sphere	12	12
Non-equivalent k-vectors for self-consistency	18	20
Non-equivalent k-vectors for DOS	364	405
Fourier coefficients for interstitial charge density	150	150

The input parameters for the calculation and space and point group symmetries are tabulated in table 2. Both space groups for δ'- as well as for ϵ-Ti_2N are non-symmorphic. Therefore, the formalism for the calculation of LAPW electron densities for non-symmorphic space groups described in [16] must be used. Essentially, the application of the space group Seitz operators (R/t_R) of table 2 instead of pure point group operators $(R/0)$, as for symmorphic space groups, leads to additional phase factors $\exp(i\boldsymbol{k}\cdot\boldsymbol{t}_R)$ in the Fourier expansion of the interstitial electron density and in the formulae for the symmetry-averaged coefficients $\bar{A}_{lm}(\boldsymbol{k}_j)$ and $\bar{B}_{lm}(\boldsymbol{k}_j)$ for the electron density inside the muffin-tin spheres (see appendix A of Marksteiner *et al* [20]).

Whereas the global crystallographic axes will be denoted by capital letters as in figures 1 and 2, small letters will be used for the local axes. It is also essential to orient the local coordinate system properly inside each muffin tin sphere, i.e. with the z-axis parallel to the rotational axis, in order to be able to use the same index picking rules (Kurki and

Table 2. Input data.

Compound	ϵ-Ti_2N	δ'-Ti_2N
Bravais type	Tetragonal primitive	Tetragonal body-centred
Space group	$P4_2/mnm$, non-symmorphic	$I4_1/amd$, non-symmorphic
Space group operations	$\{E \mid (0,0,0)\}$	$\{E \mid (0,0,0)\}$
$\{R \mid t_R\}$(+8 operations	$\{2_z \mid (0,0,0)\}$	$\{2_z \mid (0,\frac{1}{2},0\}$
$\{IR \mid t_R\}$)	$\{2_x \mid (\frac{1}{2},\frac{1}{2},\frac{1}{2})\}$	$\{2_x \mid (0,0,0)\}$
	$\{2_y \mid (\frac{1}{2},\frac{1}{2},\frac{1}{2})\}$	$\{2_y \mid (0,\frac{1}{2},0)\}$
	$\{4_3 \mid (\frac{1}{2},\frac{1}{2},\frac{1}{2})\}$	$\{4_3 \mid (\frac{3}{4},\frac{1}{4},\frac{3}{4})\}$
	$\{4_1(\frac{1}{2},\frac{1}{2},\frac{1}{2})\}$	$\{4_1(\frac{1}{4},\frac{1}{4},\frac{3}{4})\}$
	$\{m_{x\bar{y}} \mid (0,0,0)\}$	$\{m_{x\bar{y}} \mid (\frac{1}{4},\frac{3}{4},\frac{1}{4})\}$
	$\{m_{xy} \mid (0,0,0)\}$	$\{m_{xy} \mid (\frac{3}{4},\frac{3}{4},\frac{1}{4})\}$
Lattice parameter a	4.943 Å	4.149 Å
Lattice parameter c	3.036 Å	8.7858 Å
Point coordinates in multiples of a and c (with respect to origin and crystallographic axes as in figures 1 and 2)	Ti:$(u,u,0.),(1.0-u,1.0-u,0.),$ $(u+0.5,0.5-u,0.5),(0.5-u,u+0.5,0.5)$ $u=0.2961$ N: (0,0,0),(0.5,0.5,0.5)	Ti:$(0.,0.,0.25-\delta),(0.,0.,0.75+\delta),$ $(0.5,0.,\delta),(0.5,0.,0.5-\delta)$ $\delta=0.123$ Å N: (0,0,0),(0.5,0.0.25) $\square_N$:(0.,0.,0.5),(0.5,0.,0.75)
Point group symmetry	N: D_{2h} Ti: C_{2v}	N, $\square_N$: D_{2d} Ti: C_{2v}
Muffin-tin radii	R_N: 1.8338 au R_{Ti}: 2.0776 au	R_N, $R_{\square_N}$: 1.8338 au R_{Ti}: 2.0776 au

Suonio, [21]) inside each equivalent muffin-tin sphere for the proper linear combination of cubic harmonics. Whereas in δ'-Ti_2N, the local z-axis is parallel to the crystallographic Z axis for all atoms, this is not the case for ϵ-Ti_2N where the local z-axis points either in the crystallographic [110] or [$\bar{1}$10] direction. An additional rotation of the local z-axis into these directions must therefore be performed (we are actually applying the inverse operation to the k_z-axis). The tetragonal body-centred Brillouin zone for the ordered defect structure of δ'-Ti_2N and the tetragonal primitive Brillouin zone for the antirutile structure of ϵ-Ti_2N are shown in figures 3 and 4.

During the SCF cycle, the Ti 3s and 3p semicore states are treated as valence states in a second energy window.

3. Results

3.1. Band structure and eigenvalues

Figures 5 and 6 show the valence band structures of both ϵ- and δ'-Ti_2N in some k-directions of high symmetry. The names of the k points are the same as in figures 3 and 4. In table 3 band gaps, band widths and the Fermi energy with respect to either the bottom of the N 2s or the N 2p band can be found for ϵ-Ti_2N, δ'-Ti_2N, cubic, stoichiometric δ-TiN and cubic, ordered $TiN_{0.75}$ [7].

The two lowest bands of both ϵ- and δ'-Ti_2N result from overlapping N 2s states. These bands are very flat and separated by a gap of approximately 8 eV from the following six N 2p bands, which overlap the lowest Ti 3d band only in the interior of the Brillouin zone. On the surface of the Brillouin zone, all bands are twofold degenerate due to time-reversal

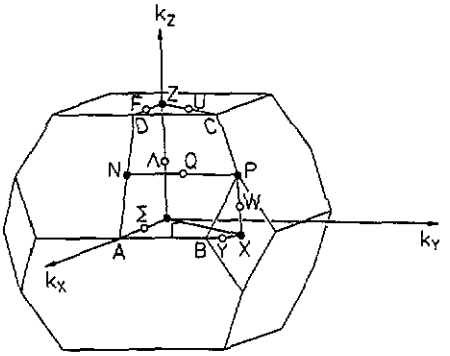

Figure 3. Brillouin zone (BZ) and irreducible wedge of the BZ (IBZ) for the tetragonal centred Bravais lattice of δ'-Ti_2N.

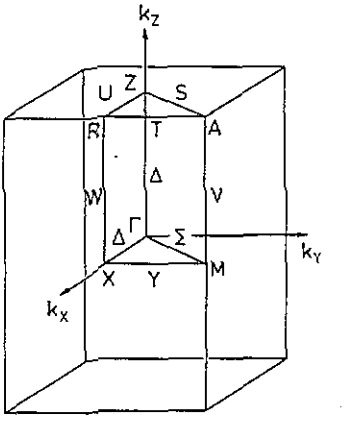

Figure 4. Brillouin zone (BZ) and irreducible wedge of the BZ (IBZ) for the tetragonal primitive Bravais lattice of ϵ-Ti_2N.

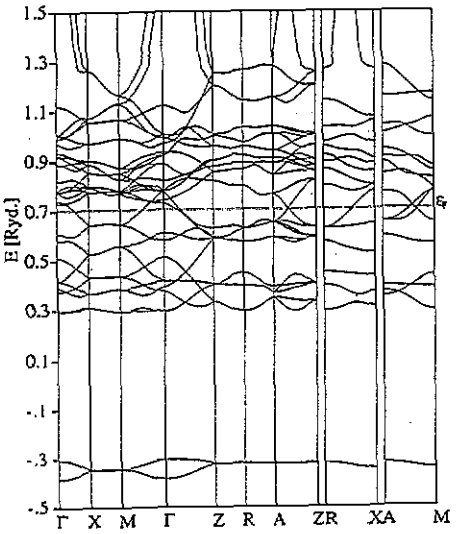

Figure 5. Band structure of ϵ-Ti_2N in some symmetry directions of k space. For the k points, the same nomenclature as in Figure 4 is used.

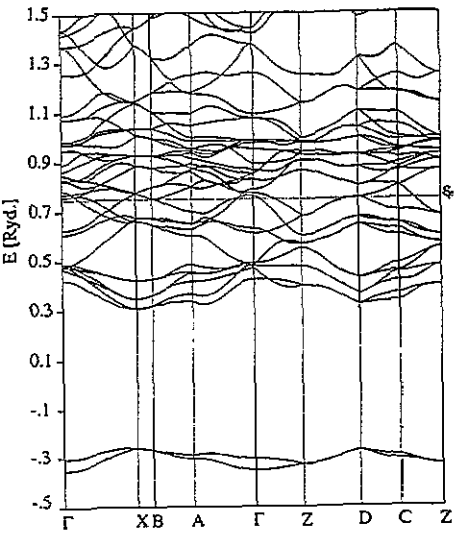

Figure 6. Band structure of δ'-Ti_2N in some symmetry directions of k space. The same nomenclature as in figure 3 is used for the k points.

symmetry. In both compounds, only the N p_z orbital (with the local z-axis pointing into the crystallographic [110] direction for ϵ-Ti_2N) can directly form p–d σ bonds with the two nearest (apical) Ti neighbours. Only three Ti–N bonds are possible per Ti atom instead of six as in cubic TiN. The 26 valence electrons occupy five Ti d bands besides the two N s and six N p bands. Both N s and p bands are narrower than in cubic δ-TiN and the gap between them is larger. In contrast, the occupied d band width has increased due to

Table 3. Band structure data in eV.

Compound	ϵ-Ti_2N	δ'-Ti_2N	δ-TiN	δ-$TiN_{0.75}$
s band width	1.1	1.20	2.45	2.12
p band width	2.35	2.97	5.48	5.11
s-p gap	8.15	7.75	6.31	6.42
Occupied d band width	3.19	3.03	2.58	2.73
Fermi level (with respect to bottom of s band)	14.78	14.95	16.83	16.39
Fermi level (with respect to bottom of p band)	5.54	6.00	8.07	7.85

the greater number of d band states below the Fermi level. The two latter effects cannot compensate, however, for the reduced s and p band width. Therefore, the Fermi level is shifted to lower energies in the heminitrides both with respect to the bottom of the s and the p band.

Table 4 presents some characteristic eigenvalues in the occupied part of the Ti d band together with their partial local (n, l) characters in a single N or Ti muffin-tin sphere and their interstitial charge fraction. For δ'-Ti_2N all tabulated states besides the state at point Γ with energy 0.6088 Ryd have large s-like charge components in the vacancy sphere, and e_g-like charge components in the Ti sphere (although the five d states are all non-degenerate for the point group symmetry C_{2v} of the Ti atoms in ϵ- and δ'-Ti_2N, the d_{z^2} and $d_{x^2-y^2}$ states are still characterized as e_g-like and the d_{xy}, d_{xz} and d_{yz} states as t_{2g}-like). However, the vacancy charge is smaller than in the case of the hypothetically ordered $TiN_{0.75}$ [7], where we referred to analogous states as so-called 'vacancy' states. In the case of δ'-Ti_2N, the Ti atoms are shifted away from the vacancy in the Z-direction. Besides increasing the vacancy–Ti distance in the Z-direction, the Ti atoms also get out of plane with the vacancies in the X- and Y-direction. Therefore, the superposition of the tails of the Ti d functions furnishes less charge in the unoccupied N muffin-tin sphere than in $TiN_{0.75}$. e_g-like and t_{2g}-like Ti bands overlap in the interior of the Brillouin zone explaining the t_{2g}-like character of the energetically lower d band state at $k = \Gamma$ with an energy of 0.6088 Ryd. With one exception, the N p character of these states is low. Ti d and N p bands overlap only slightly and only near Γ. The higher amount of N p charge for the d band state at k=(001) (point Z) can be explained by the overlap of N p and Ti d bands in the direction Γ–Z.

For ϵ-Ti_2N, the N p bands overlap in the interior of the Brillouin zone more strongly with the lowest Ti d bands producing also a larger amount of N p charge for the states at the bottom of the d band. The antirutile structure of ϵ-Ti_2N enables Ti e_g-like states to form (weak) Ti–Ti d–d σ bonds as well as N–Ti p–d σ bonds in the (001) plane. Consequently, these bonding states are stabilized and lowered in energy. They are thus found at the bottom of the d and p band, respectively. t_{2g}-like Ti d states are only involved in weaker π bonding with either N p or Ti d states and have, therefore, higher energies than the e_g-derived bonding p–d σ and d–d σ states.

3.2. Densities of states (DOS) and partial local densities of states

Figure 7 shows the DOS of (*a*) ϵ- and (*b*) δ'-Ti_2N calculated by means of the tetrahedron method of Lehmann and Taut [19]. The first and second DOS peaks are called the s and p bands because N s and p states, respectively, are predominantly contributing to them. The s and p bands are narrower for ϵ- than for δ'-Ti_2N. For ϵ-Ti_2N, the s band extends from -1.09 to -1.01 Ryd below the Fermi energy E_F, the p band from -0.41 to -0.24 Ryd

Table 4. Characteristic eigenvalues and (n, l) characters of δ'-Ti_2N and ϵ-Ti_2N.

k	E	q_{out}	N full		N empty		Ti								
			p	tot	s	tot	s	p	d	tot	d_{z^2}	$d_{x^2-y^2}$	d_{xy}	d_{xz}	d_{yz}
						δ'-Ti_2N									
(000)	0.6088	35.6		1.0		0.6			15.3	15.3			15.3		
	0.6279	35.8			11.3	11.3			12.4	12.4	6.0	6.4			
$(\frac{1}{2},\frac{1}{2},0)$	0.6724	45.9	1.4	1.9	8.4	9.2	0.4	1.7	5.9	8.0	2.0	2.1	1.1	0.4	0.2
$(0,0\frac{1}{2})$	0.5901	33.1	0.3	0.4	10.9	11.2	0.9	0.3	9.8	10.9	5.0	4.8			
$(\frac{1}{2},\frac{1}{2},\frac{1}{2})$	0.6834	48.2	1.3	1.7	8.9	9.6	0.3	2.1	5.0	7.3	1.4	1.4	1.0	0.4	0.8
(001)	0.5694	28.4	7.4	7.5	9.0	9.0	0.6	0.3	8.8	9.7	5.3	3.5			
						ϵ-Ti_2N									
(000)	0.5804	42.4		1.2				0.5	13.4	13.8	3.3	10.0			
	0.6118	80.4		0.4				2.7	2.0	4.7				2.0	
(100)	0.5258	54.4	4.5	5.1			0.5	0.7	7.7	8.9	4.0	3.5		0.2	
	0.6442	35.1	1.8	2.6				0.3	14.6	14.9	3.8	7.0		3.8	
(110)	0.5609	47.9	5.5	5.5			0.2	0.4	9.7	10.3	1.6	7.5		0.7	
	0.6478	38.3		1.2			0.4	0.3	14.1	14.8	7.5	6.6			
(001)	0.5886	50.8	2.6	2.8			0.4	0.6	10.0	10.9	2.9	6.2			0.85
	0.5927	50.0		0.5				0.8	11.5	12.3			10.2	1.3	
	0.6312	39.6	0.4	1.2				0.7	13.9	14.5				7.8	6.1
(111)	0.5926	37.2	8.5	8.6			0.2		11.0	11.4	5.1	3.4	2.5		
	0.6514	31.3		0.6					16.9	16.9			10.2	5.7	
	0.6525	57.7	1.0	1.8				2.1	7.7	9.8				3.1	4.6

below E_F, whereas for δ'-Ti_2N the s band goes from -1.10 to -1.01 Ryd and the p band from -0.44 Ryd to -0.22 Ryd below E_F. The d band with mainly Ti 3d states extends from -0.41 Ryd (-0.44 Ryd) below E_F to 0.36 Ryd (0.35 Ryd) above E_F for ϵ- (δ')-Ti_2N.

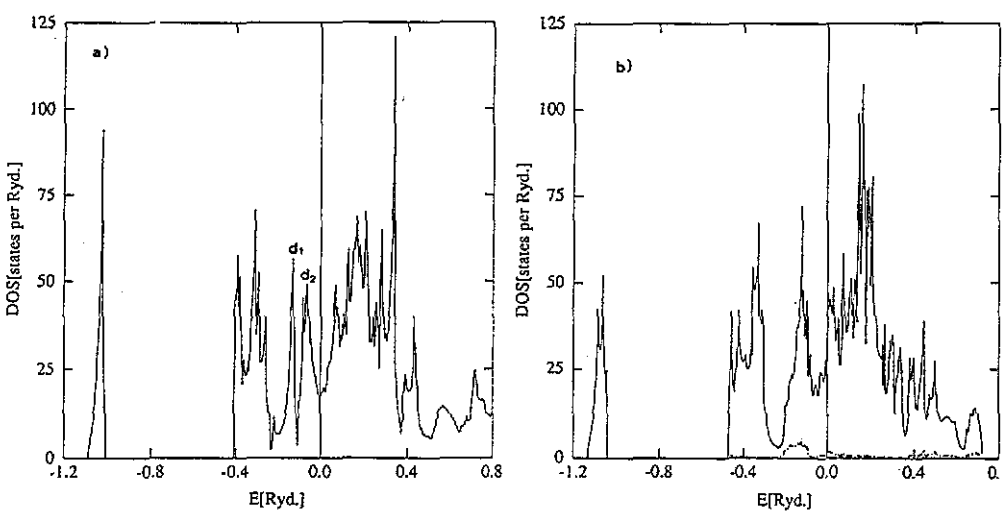

Figure 7. Density of states of (a) ϵ- and (b) δ'-Ti_2N in states of one spin direction per Rydberg and unit cell. For δ'-Ti_2N, the local vacancy DOS is plotted as the dash-dotted curve.

The main difference between the DOS of ϵ- and δ'-Ti_2N is found at the bottom of the d band which is separated by a distinct minimum from the p band. Two peaks, d_1 and d_2, separated by a sharp minimum at -0.11 Ryd below E_F are characteristic for the energetically lower part of the d band of ϵ-Ti_2N, whereas in δ'-Ti_2N, only one d band peak with its maximum at -0.1 Ryd is found below E_F. The Fermi level for ϵ-Ti_2N lies in the DOS minimum above the peak d_2. For δ'-Ti_2N, the Fermi level is situated in the ascent of the main DOS d band peak just after a DOS minimum. If the Fermi level were shifted to this minimum and the states of δ'-Ti_2N were occupied according to the rigid-band model it would refer to a titanium nitride of composition $Ti_2N_{0.98}$ very near to the composition Ti_2N of the ideal δ'-phase.

For disordered $TiN_{0.5}$ the Fermi level is found in the broad first maximum of the d band DOS [9]. In stoichiometric TiN [7] no separate peak is found at the bottom of the d band and E_F lies in the ascent of the d band whereas in ordered $TiN_{0.75}$ a sharp peak from so-called 'vacancy' states appears at the bottom of the d band but is only half occupied.

If one uses the position of the Fermi level of a structure as a criterion for its stability, then disordered $TiN_{0.5}$ should be unstable compared to both ϵ-Ti_2N and δ'-Ti_2N, and ϵ-Ti_2N should be more stable than δ'-Ti_2N as is indeed found experimentally. The occurrence of the ϵ-phase just for $x = 0.5$ can be explained by the position of the Fermi level in a very sharp DOS minimum. For the disordered phase, TiN_x, E_F is situated in a broad maximum for compositions near $x = 0.5$, but shifts also to a minimum for $x = 0.58$ [9] indicating increased stability of the disordered δ-TiN_x phase at higher N contents, but relative instability with respect to both, ϵ- and δ'-Ti_2N, for compositions around $x = 0.5$. The situation is opposite for the hypothetically ordered $TiN_{0.75}$ [7] with the Fermi level situated in the very unfavourable position of a sharp DOS maximum destabilizing the hypothetically ordered compound compared to disordered $TiN_{0.75}$. All calculations refer to a temperature of $0K$. However, for the Ti–N system equilibrium conditions are only fulfilled for higher temperatures because of the low N diffusion rate at low temperatures.

ϵ-Ti_2N is also experimentally the most stable phase for a N content of $x = 0.5$, but a high activation energy seems to be necessary for its formation, explaining why the phase transformation from the δ'-Ti_2N and from the δ-TiN_x phase to the ϵ-phase occur only at higher temperatures [11].

In the hypothetically, ordered defect structure of $TiN_{0.75}$ [7], the integration of the DOS from the bottom to the top of the Ti d band gives a charge corresponding to a number of electrons larger by two than the possible number of Ti 3d electrons. Therefore, we concluded that one so-called 'vacancy state' per unit cell must contribute to the Ti d band of ordered $TiN_{0.75}$ [7]. For δ'-Ti_2N, however, the same integral corresponds exactly to the charge of the possible number of Ti 3d electrons and there is no explicit contribution of 'vacancy' states. One reason might be the relaxation of the Ti atoms away from the vacancy which reduces the amount of charge in the vacancy sphere, resulting from the overlapping tails of the nearest neighbour Ti 3d functions. Indeed, only half an electron is localized in the vacancy sphere of δ'-Ti_2N compared to 0.7 electrons for ordered $TiN_{0.75}$ [7], as can be seen in table 5, where partial local band charges and partial local valence electron charges are displayed for ϵ-Ti_2N and δ'-Ti_2N. The charge distribution is very similar for both heminitrides. Compared to stoichiometric TiN, where the Ti atoms are surrounded by six instead of three N atoms, less charge is found in the p and more in the d band, and the percentage of p-like nitrogen charge in the d-band is greatly reduced in both heminitrides. One must also take into account for this comparison the different size of the muffin-tin spheres, with the N sphere being smaller and the Ti sphere bigger in the heminitrides than in δ-TiN or $TiN_{0.75}$ [7].

Table 5. Partial local charges in the Ti, N and N vacancy ($\square_N$) sphere in electrons per muffin-tin sphere, and local charge in the interstitial region between the muffin-tin spheres (int.) in electrons per formula unit.

Band		ϵ-Ti_2N			δ'-Ti_2N			
		Ti	N	int.	Ti	N	$\square_N$	int.
s band	s	0.02	1.51		0.01	1.51		
	p	0.02			0.02			
	d	0.03			0.03			
	total	0.07	1.51	0.32	0.07	1.51		0.35
p band	s	0.08	0.01		0.07	0.01	0.05	
	p	0.08	2.86		0.08	2.88	0.01	
	d	0.46			0.47			
	total	0.63	2.88	1.86	0.64	2.91	0.07	1.86
occ.	s	0.02			0.02	0.01	0.37	
d band	p	0.05	0.28		0.05	0.27	0.08	
	d	1.18	0.04		1.18	0.04	0.02	
	total	1.26	0.33	2.16	1.22	0.31	0.47	2.23
occ.	s	0.12	1.53		0.11	1.52	0.42	
valence	p	0.15	3.15		0.15	3.15	0.09	
bands	d	1.68	0.04		1.68	0.05	0.02	
	total	1.96	4.72	4.36	1.93	4.73	0.53	4.34

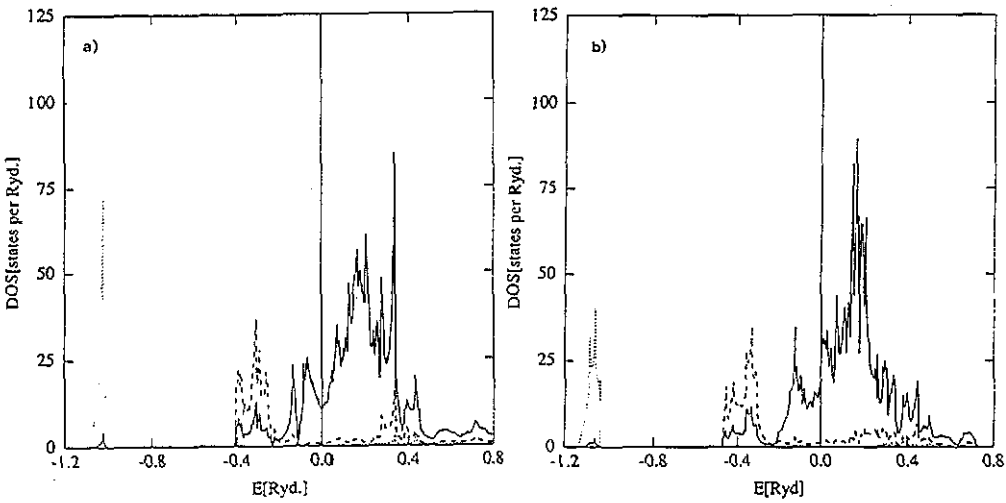

Figure 8. Partial local N s (dotted), N p (dashed) and Ti d (full line) DOS of (a) ϵ- and (b) δ'-Ti_2N. Same units as in figure 7.

Figure 8 shows the partial Ti 3d and N 2s and 2p DOS for both, ϵ- (a) and δ'- (b) Ti_2N. The p band contains the bonding N p-Ti d states. Therefore, about one third of the p band DOS for both compounds comes from Ti d states. Because of the low number of only three nearest N neighbours for one Ti atom, the N p DOS in the Ti d band is low for both heminitrides. Some N p DOS is found at the top of the d band where the antibonding p–d states are situated, and there is also a small N p DOS contribution to the first d band peak of ϵ-Ti_2N.

Further information on the bonding and antibonding interactions generating special structures in the DOS can be found from the split of the Ti 3d and N 2p states in the crystal field of their nearest neighbours, which is of C_{2v} symmetry for the Ti atoms in both compounds, and of D_{2h} (D_{2d}) symmetry for N in ϵ (δ')-Ti_2N. Thus, the five Ti 3d states of both compounds as well as the three N 2p states of δ'-Ti_2N are non-degenerate, whereas for ϵ-Ti_2N, the N p_x and p_y states remain degenerate. The p band is less split and narrower for ϵ- than for δ'-Ti_2N. For ϵ-Ti_2N, only the N p_z states form σ bonds with the Ti d_{z^2} states in the (001) plane. These states have, therefore, a lower energy than the other p–d bonding states and are responsible for the sharp peak at the bottom of the p band.

A more thorough discussion about chemical bonding in both heminitrides, especially about Ti–Ti d–d bonding, will be possible after having presented electron density contour plots.

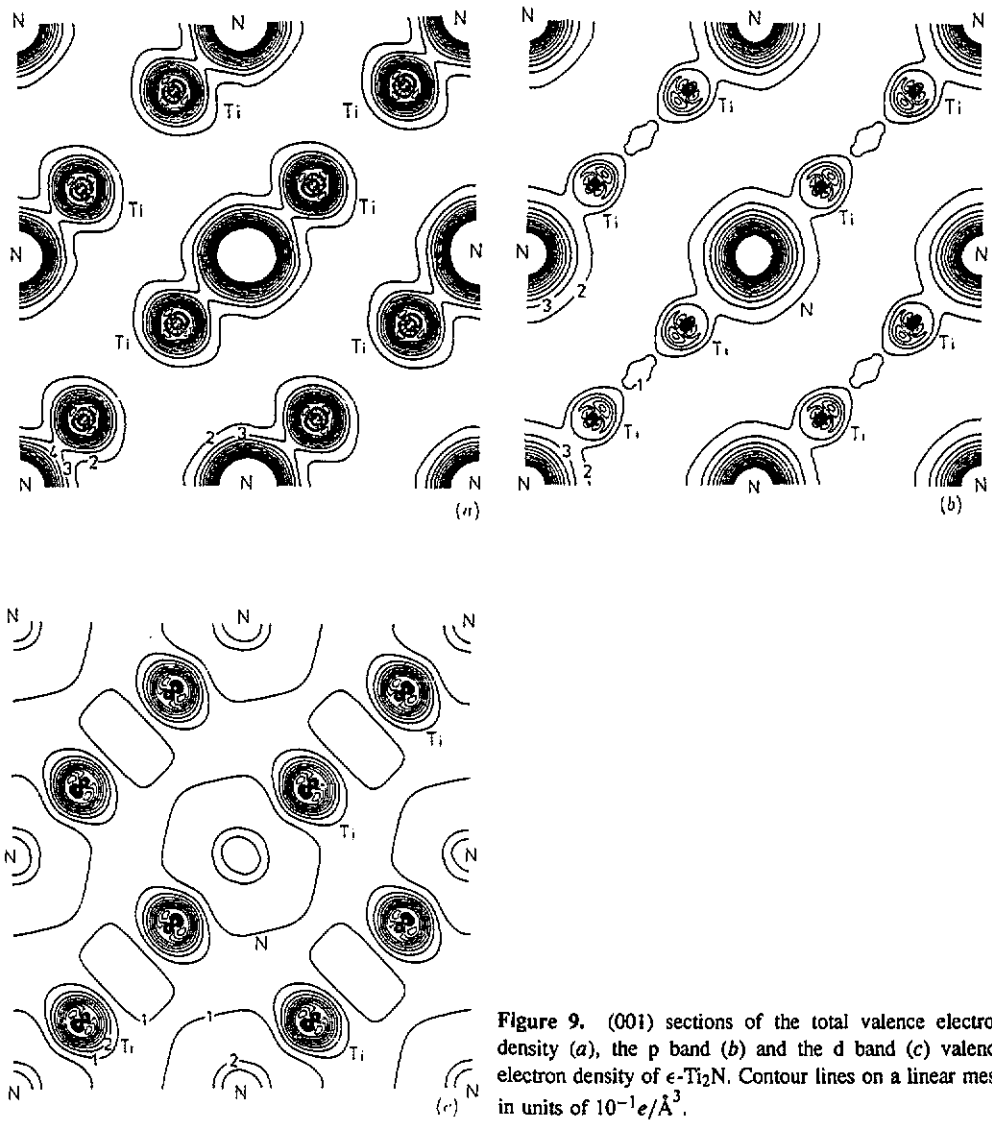

Figure 9. (001) sections of the total valence electron density (*a*), the p band (*b*) and the d band (*c*) valence electron density of ϵ-Ti_2N. Contour lines on a linear mesh in units of $10^{-1}e/Å^3$.

3.3. Electron density

Electron density contour plots have been obtained for both compounds by integrating over all valence states (total valence electron density) or by integrating only over all states of a particular band in the DOS (p band or d band electron density). For ϵ-Ti_2N, the d band electron density was further split into the contribution of the first and second d band peak (subbands d_1 and d_2).

For ϵ-Ti_2N, we calculated contour plots for a (001) section (XY plane) and for a (110) section, whereas for δ'-Ti_2N, we chose the (001) and the (010) section (XY and XZ plane).

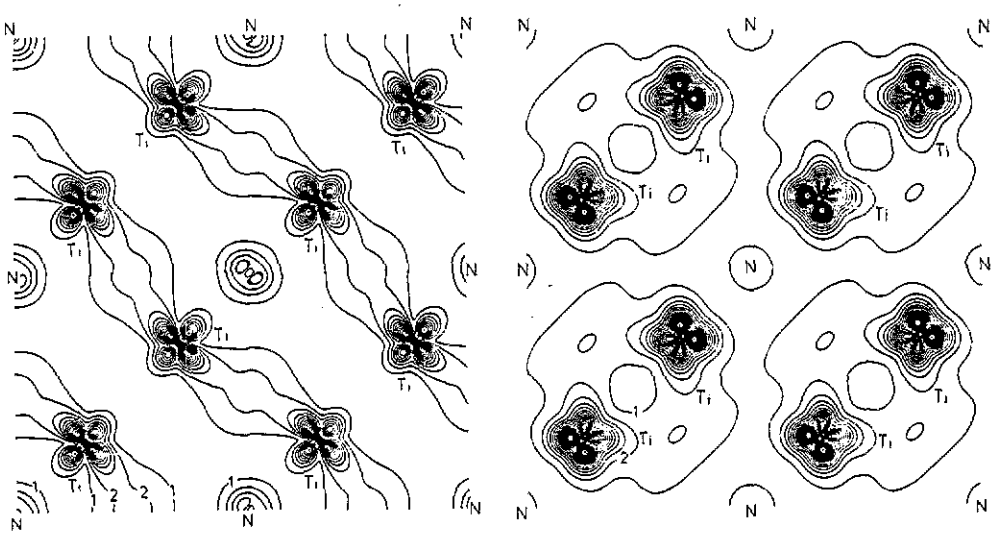

Figure 10. (001) sections of the d_1 subband (left)and d_2 subband (right) valence electron density of ϵ-Ti_2N. Contour lines on a linear mesh in units of $0.05e/Å^3$.

Let us discuss first the (001) sections of ϵ-Ti_2N. Figure 9 shows electron density contour plots in the (001) plane for all occupied valence states and, separately, for the p band and d band states of ϵ-Ti_2N. One clearly recognizes the strong p–d σ bonds between N p_z and Ti d_{z^2} states between each nitrogen atom and its two nearest (apical) titanium neighbours in the (001) plane, which are visible both in the total and the p band electron density. The local z-axis is pointing into the crystallographic [110] direction. All Ti_2N units are aligned in the [110] direction in the basal plane. Parallel adjacent Ti_2N units are only connected by weak Ti–Ti d–d σ bonds of e_g-like states in the $[\bar{1}10]$ direction at right angles to the orientation of the Ti_2N units. The overall Ti electron density is e_g-like in the (001) plane. In the (XY) plane at $Z = 0.5c$ the Ti_2N units are oriented in the $[\bar{1}10]$ direction and the d–d σ bonds point into the [110] direction.

In order to analyse the d–d bonds we display in figure 10 the contour plots for the contribution of subbands d_1 and d_2 to the valence electron density in the (001) plane. The eigenstates of band d_1 produce an e_g-like charge density with distinct Ti–Ti d–d σ bonds in the $[\bar{1}10]$ direction (figure 10, left). Band d_1 accommodates four electrons (one per Ti atom). In ϵ-Ti_2N, Ti e_g-like states can undergo either N–Ti p–d σ or Ti–Ti d–d σ bonds in the (001) plane. The corresponding bonding states are found at the bottom of either the p or d band. The small N p contribution to subband d_1 can be explained by N p–Ti e_g mixing.

The subband d_2 accommodates six electrons and corresponds obviously to t_{2g}-like Ti d states with no contribution of N p states. In the antirutile structure, the t_{2g}-like Ti states cannot form p–d σ bonds in the (001) plane, but they are involved in d–d π bonding as can also be seen from figure 10 (right).

The contour plots of the valence electron and the p band electron density of ϵ-Ti_2N in the (110) plane (figure 11, top and centre) show the Ti_2N units in subsequent (001) planes to be interconnected by strong N p–Ti d bonds. The d band electron density in the (110) plane (figure 11, bottom) can again be split into the contribution of the states in the peaks d_1 and d_2 (figure 12). The d_1 band does not contribute to d–d bonding in the (110) plane (figure 12, bottom) but the contour plot for the d_2 band shows the t_{2g}-like Ti d states to be involved in d–d π bonding with Ti atoms in adjacent (110) planes (figure 12, top).

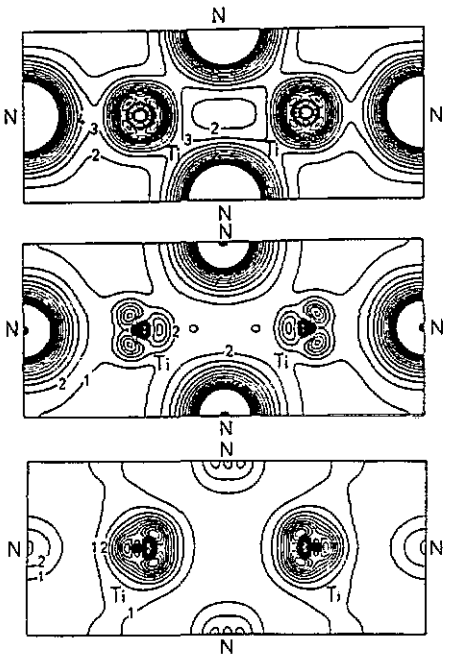

Figure 11. (110) sections of the total (top), the p band (centre) and the d band (bottom) valence electron density of ϵ-Ti_2N. Contour lines on a linear mesh in units of $10^{-1}e/Å^3$.

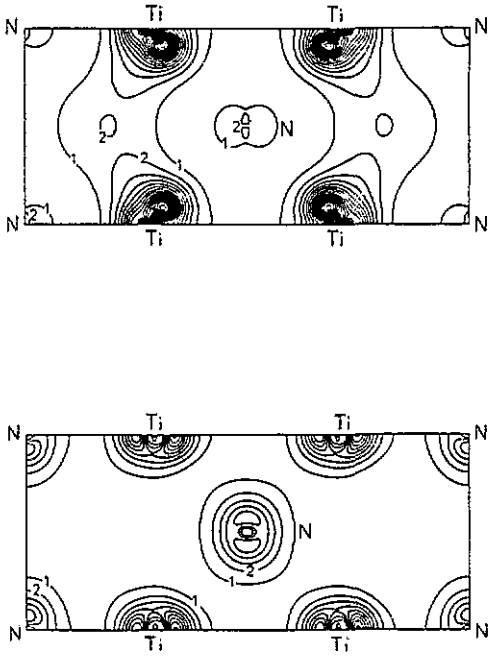

Figure 12. (110) sections of the d_1 subband(bottom) and d_2 subband (top) valence electron density of ϵ-Ti_2N. Contour lines on a linear mesh in units of $0.05e/Å^3$.

The electron density contour plot for δ'-Ti_2N in the (001) plane (figure 13, top: all valence states; centre: p band states) shows p–d σ bonds between the N atoms and the four Ti atoms surrounding each N atom in the (001) plane (actually, the Ti atoms are shifted by ± 0.123Å out of the (001) plane). The Ti charge density (figure 13, bottom: d band states) has e_g-like symmetry as in ordered $TiN_{0.75}$ [7], but, in contrast to the latter compound, not much bonding can be recognized between these e_g-like states on the Ti atoms adjacent to the vacancy. The reason might be that the relaxation of the Ti atoms away from the vacancy in the Z-direction has reduced the d–d overlap in δ'-Ti_2N significantly.

Inspection of the electron density contour plots of δ'-Ti_2N in the (010) plane (figure 14, top: all valence states; bottom: d band states) shows, nevertheless, some weak octahedral

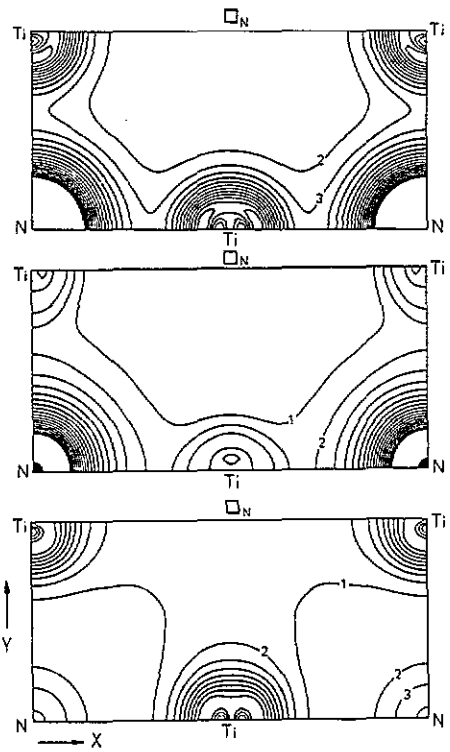

Figure 13. (001) sections of the total (top), the p band (centre) and the d band (bottom) valence electron density of δ'-Ti_2N. Contour lines on a linear mesh in units of $10^{-1}e/Å^3$.

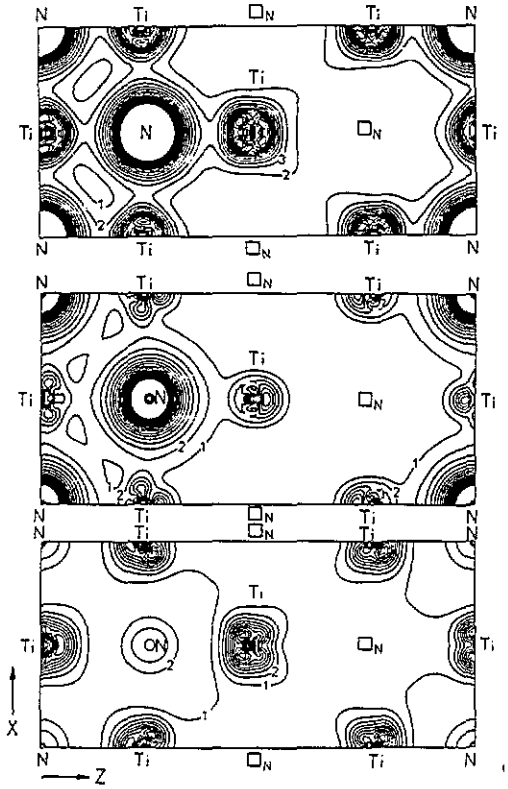

Figure 14. (010) sections of the total (top), the p band (centre) and the d band (bottom) valence electron density of δ'-Ti_2N. Contour lines on a linear mesh in units of $10^{-1}e/Å^3$.

d–d σ bonds between the Ti atoms surrounding the vacancy (see also figure 16). The charge density of the Ti atoms surrounding the vacancy is t_{2g}-like in this plane whereas it is still e_g-like for the Ti atoms surrounded by three N neighbours and consequently forming TiN p–d σ bonds (figure 14, centre). For this section we have a ribbon-like structure of rows of Ti_2N units with the ribbons only connnected by the weak octahedral bonds. Shifting of every second row and rotating it by 90° would lead to the more stable structure of ϵ-Ti_2N, but a high activation energy is necessary for this transformation. Indeed, the formation of ϵ-Ti_2N by N implantation of Ti films is found to be kinetically hindered at the appropriate N concentration [13], and the transformation of the δ'- into the ϵ-phase is also only possible at higher temperatures [11].

It is also interesting to plot charge density contour plots for individual states. For ϵ-Ti_2N, we show in figure 15 such a contour plot in the (110) plane for the state Γ_1 with energy 0.5804 Ryd, belonging to the band d_1. The plot shows that it is an e_g-like Ti d state forming Ti–Ti d–d σ bonds at right angles to the bond direction of the Ti_2N units.

For δ'-Ti_2N, we show in the figures 16 and 17 contour plots for two different states at $\boldsymbol{k} = \Gamma$. In figure 16 we display a contour plot in the (001) plane of the state $\Gamma_{1'}$ with $E = 0.6088$ Ryd, which shows a t_{2g}-like state forming d–d σ bonds between the Ti atoms octahedrally surrounding a vacancy. For the state $\Gamma_{3'}$ with $E = 0.6279$ Ryd we have

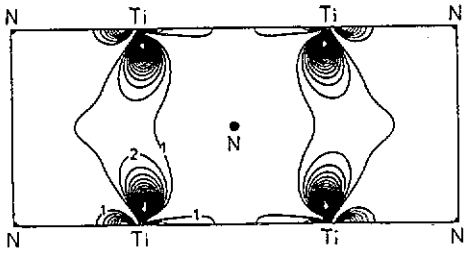

Figure 15. (110) section of the valence electron density of the state Γ_1 of ϵ-Ti_2N with energy 0.5804 Ryd. Contour lines on a linear mesh in units of $0.05e/Å^3$.

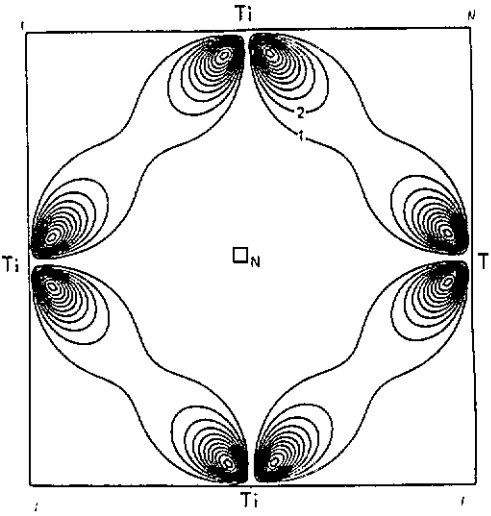

Figure 16. (001) section of the valence electron density of the state $\Gamma_{1'}$ of δ'-Ti_2N with energy 0.6088 Ryd. Contour lines on a linear mesh in units of $0.05e/Å^3$.

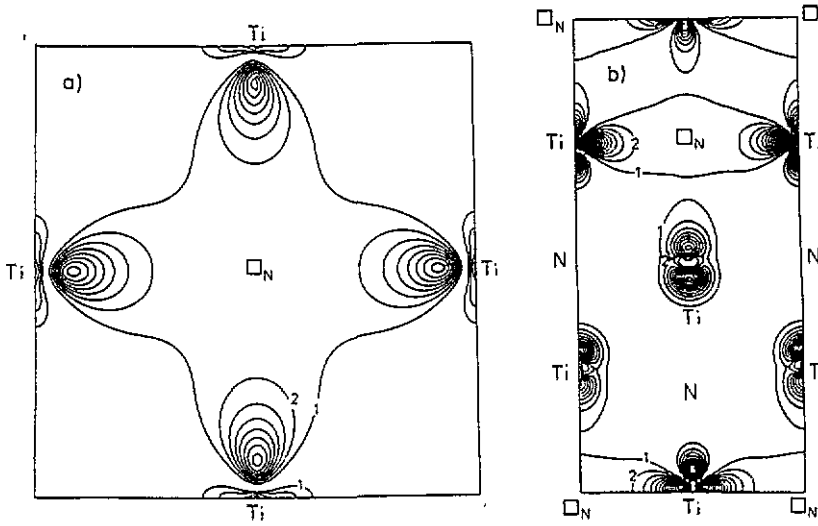

Figure 17. (*a*) (001) and (*b*) (010) section of the valence electron density of the state $\Gamma_{3'}$ of δ'-Ti_2N with energy 0.6279 Ryd. Contour lines on a linear mesh in units of $0.05e/Å^3$.

calculated contour plots in both the (001) (a) and the (010) (b) plane which can be seen in figure 17. This state is an e_g-like Ti state and would correspond to a so-called vacancy state of hypothetically $TiN_{0.75}$ [7] , but in contrast to $TiN_{0.75}$, only very weak d–d σ bonding across the vacancy can be found for this state, because of the larger vacancy–Ti distance.

4. Summary

Even without a proper discussion of energetics, which will be found in a second paper [14], the comparison of the present band structure results, such as densities of states and charge densities, furnishes a satisfying explanation for the occurrence of the metastable [11] superstructure of δ'-Ti_2N in the Ti–N phase diagram as well as for the high stability of the ϵ-phase.

In δ'-Ti_2N, the arrangement of vacancies enables the t_{2g}-like states of the Ti atoms surrounding the vacancies to form octahedral d–d σ bonds. The octahedral bonding Ti t_{2g}-like states are thus lowered in energy and form a separate peak at the bottom of the d band separated by a minimum from the rest of the band. The Fermi level moves from the first d band DOS peak in disordered TiN_x (x near 0.5) [9] to a position slightly above this minimum which, assuming the rigid-band model to be valid, corresponds to a titanium nitride of composition $Ti_2N_{0.98}$, thus very near the ideal composition Ti_2N of the δ'-phase. In contrast to the results for hypothetically ordered $TiN_{0.75}$ [7], the overlap of the e_g-like states localized at the Ti atoms adjacent to the vacancies is rather small if these Ti atoms are assumed to be shifted away from the vacancies towards the remaining N atoms in the Z-direction parallel to the crystallographic c-axis. Therefore, there occurs no significant d–d bonding of Ti e_g-like states across the vacancy. The Ti electron density has t_{2g}-like symmetry towards the three vacancy 'neighbours' but e_g-like symmetry towards the three N neighbours.

The transformation to ϵ-Ti_2N enables Ti e_g-like states to enter not only in N–Ti p–d σ but also in Ti–Ti d–d σ bonding in the basal plane between strongly bound 'molecular' Ti_2N units. The corresponding states are thus stabilized and form a sharp peak (subband d_1) at the bottom of the d band. This is obviously the main reason for the stabilization of the ϵ-phase with respect to the δ'-phase. The Fermi level moves to a sharp DOS minimum after the second d band peak (subband d_2) of t_{2g}-like Ti d states which are energetically lowered by d–d π bonding. The Ti electron density shows t_{2g}-like symmetry in the (110) plane but e_g-like symmetry in the (001) plane.

All calculations refer to 0 K. Temperature effects should be small for the quantities discussed in the present paper, i.e. the band structure, DOS and electron density. The lattice expansion with increasing temperature could lead to slightly narrower bands and the temperature-dependent Fermi factors describing the occupation of electronic states near the Fermi level could cause some smearing of the density of states. As the Fermi level lies in or very near a minimum of the DOS for both compounds, the latter effect should not be too important, either.

Unfortunately, no spectra are available for either ϵ- nor δ'-Ti_2N to check the results of the present band structure calculation. We wish to encourage experimentalists to perform such measurements.

Acknowledgments

I want to thank Professor Neckel for many discussions and his constant interest in this work. I gratefully acknowledge the financial support of the Hochschuljubiläumsstiftung der Stadt Wien and the assistance of the Vienna University Computer Center where the calculations were performed.

References

[1] Ehrlich P 1949 *Z. Anorg. Chem.* **259** 1
[2] Molarius J M, Korhonen A S and Ristolainen E O 1985 *J. Vac. Sci. Technol.* **A3** 2419
Wriedt H A and Murray J L 1987 *Bull. Alloy Phase Diagrams* **8** 378
[3] Lobier G and Marcon J P 1969 *C.R. Acad. Sci.* C **268** 1132
[4] Nagakura S and Kusunoki T 1977 *J. Appl. Crystallogr.* **10** 52
[5] Christensen A N, Alamo A and Landesman J P 1985 *Acta Crystallogr.* **C41** 1009
[6] Neckel A, Rastl P, Eibler R, Weinberger P and Schwarz K 1976 *J. Phys. C: Solid State Phys.* **9** 579
[7] Herzig P, Redinger J, Eibler R and Neckel A 1987 *J. Solid State Chem.* **70**, 281
[8] Klima J, Schadler G, P Weinberger and Neckel A 1985 *J. Phys. F: Met. Phys.* **15** 1307
[9] Marksteiner P, Weinberger P, Neckel A, Zeller R and Dederichs P H 1986 *Phys. Rev.* B **33** 812
[10] Lengauer W and Ettmayer P 1987 *High Temp.–High Press.* **19** 673
[11] Etchessahar E, Young-Un Z Sohn, Hamelin M and Debuigne J 1991 *J. Less-Common Met.* **167** 261
[12] Holmberg B 1962 *Acta Chem. Scand.* **16** 1255
[13] Zhou X, Dong H K, Li H D and Liu B X 1988 *J. Appl.Phys.* **63**, 4942
[14] Eibler R and Vackář J to be published
[15] Andersen O K 1975 *Phys. Rev.* B **12** 3060
[16] Koelling D D and Arbmann G O, 1975 *J. Phys. F: Met. Phys.* **5** 2041
[17] Schlapansky F, Herzig P, Eibler R, Hobiger G and Neckel A, 1989 *Z. Phys.* B **75** 187
[18] Hedin L and Lundqvist S 1972 *J. Physique Coll.* C **3** 33
[19] Lehmann G and Taut M 1972 *Phys. Status Solidi* b **54** 469
[20] Marksteiner P, Blaha P and Schwarz K 1986 *Z. Phys.* B **64**, 119
[21] Kurki-Suonio K 1977 *Israel J. Chem.* **16**, 115